

Ion-ion kink instability in the magnetotail:

1. Linear theory

H. Karimabadi,¹ W. Daughton,² P. L. Pritchett,³ and D. Krauss-Varban¹

Received 7 May 2003; revised 30 June 2003; accepted 12 August 2003; published 18 November 2003.

[1] A number of different ion species are known to exist in the magnetotail. In particular, cold lobe ions and current-carrying hot plasma sheet ions are a permanent feature of the magnetotail and result in various types of instabilities. One such instability is the ion-ion kink mode. Detailed properties of this mode in the magnetotail are investigated in a two series paper using a combination of linear Vlasov theory, three-dimensional (3-D) full particle and hybrid (fluid electron, kinetic ions) simulations. Here we consider the linear properties of the mode in detail. Although the mode shows similarities to a velocity driven instability, its linear mode properties do exhibit dependencies on the kinetic details of the secondary ion population.

INDEX TERMS: 2744 Magnetospheric Physics: Magnetotail; 2772 Magnetospheric Physics: Plasma waves and instabilities; 7843 Space Plasma Physics: Numerical simulation studies; *KEYWORDS:* kink mode, magnetotail instabilities, linear theory, Kelvin-Helmholtz instability, Vlasov theory

Citation: Karimabadi, H., W. Daughton, P. L. Pritchett, and D. Krauss-Varban, Ion-ion kink instability in the magnetotail: 1. Linear theory, *J. Geophys. Res.*, 108(A11), 1400, doi:10.1029/2003JA010026, 2003.

1. Introduction

[2] Thin current sheets are frequently observed both in the magnetotail and the magnetopause. In the magnetotail, thin current structures form during the growth phase of substorms [Kaufmann, 1987; McPherron *et al.*, 1987; Mitchell *et al.*, 1990; Sergeev *et al.*, 1990; Lin *et al.*, 1991; Pulkkinen *et al.*, 1992; Sergeev *et al.*, 1993; Lui, 1993]. The half thickness of these current structures can be as small as the ion collisionless skin depth c/ω_{pi} or the ion gyroradius ρ_i based on the asymptotic lobe field. These two lengths are roughly equal in the central plasma sheet where $T_i \gg T_e$. It is believed that these structures can extend over considerable radial distances in the tail [Pulkkinen *et al.*, 1999]. Thin current structures on the ion scale have also been observed at the dayside magnetopause [e.g., Song *et al.*, 1993; Russell, 1995].

[3] The existence of such thin current structures greatly augments the growth rates of various current sheet instabilities. Examples include the collisionless ion tearing instability [Schindler, 1974; Galeev and Zelenyi, 1976], the lower hybrid drift instability (LHDI) [Davidson and Gladd, 1975; Huba *et al.*, 1977, 1980], the kinetic cross-field current instability [Lui *et al.*, 1990, 1991], the ion-Weibel instability [Chang *et al.*, 1990], the ballooning instability [Roux, 1985; Miura *et al.*, 1989; Roux *et al.*, 1991], the electron shear flow instability [Drake *et al.*,

1994, 1997], Kelvin-Helmholtz instability [Yoon *et al.*, 1996], and the drift kink instability [Zhu and Winglee, 1996; Ozaki *et al.*, 1996; Pritchett *et al.*, 1996].

[4] The drift kink mode is driven by the relative streaming between the electrons and ions. The properties of this mode were originally derived from particle-in-cell simulations which assumed quite small values of the ion to electron mass ratio, $m_i/m_e \leq 25$ [Zhu and Winglee, 1996; Pritchett *et al.*, 1996] or included a substantial nondrifting background plasma component [Ozaki *et al.*, 1996]. Raising m_i/m_e to ~ 100 , however, resulted in a significant decrease in the observed growth rate [Hesse and Birn, 2000], and a complete Vlasov analysis of the linear theory for the mode in a one-dimensional (1-D) Harris current sheet [Daughton, 1998, 1999] demonstrated that the growth rate continues to fall rapidly out to realistic values of $m_i/m_e = 1836$ where $\gamma/\Omega_{ci} \sim 0.003$.

[5] Daughton [1999] noted, however, that a large growth rate $\gamma/\Omega_{ci} \sim 0.1$ would still exist for a kink mode if the two streaming populations involved separate ion species. This mode was also reported in hybrid simulations of the magnetotail [Krauss-Varban and Omidi, 1996; Krauss-Varban and Karimabadi, 2003]. The presence of a separate, stationary ion population introduces an effective shear into the net ion velocity profile, and so this mode has some of the properties of a Kelvin-Helmholtz (K-H) mode. We refer to this instability as the ion-ion kink mode. In the magnetotail the presence of the secondary ion population can be due to the lobe plasma or due to ionospheric ions. Similarly, at the magnetopause there exist several sources of secondary ions that can give rise to the ion-ion kink instability. Examples include (1) cold ionospheric ions and (2) reflected ions [Fuselier, 1995].

[6] Given the expected prevalence of the ion-ion kink mode in the magnetotail and at the magnetopause, it is

¹Department of Electrical and Computer Engineering, University of California, San Diego, La Jolla, California, USA.

²Los Alamos National Laboratory, Los Alamos, New Mexico, USA.

³Department of Physics and Astronomy, University of California, Los Angeles, Los Angeles, California, USA.

important to develop a better understanding of this instability and determine its observable signatures. Recent evidence [e.g., *Sergeev et al.*, 2003; *Volwerk et al.*, 2003] for the presence of the kink mode in the magnetotail provides added impetus for this research. Despite its importance, many salient features of the ion-ion kink instability have remained poorly understood. For instance, there is no consensus as to the driving mechanism for the instability. Is it the velocity shear much like the Kelvin-Helmholtz instability, or is it the relative drift between the two ion populations that drives the instability? The saturation mechanism of the instability also remains poorly understood. The goal of this series of two papers is to examine the linear and nonlinear properties of the ion-ion kink instability in detail and use realistic parameters and simulations in order to predict the observable signatures of this instability in the magnetotail. To this end, we have used a combination of linear Vlasov theory, full particle, and hybrid (electron fluid, kinetic ions) simulations for a wide range in parameter space. In this paper we discuss the linear properties of the ion-ion kink mode in detail. These results will be used, in conjunction with the simulations by *Karimabadi et al.* [2003, hereafter referred to as Paper II], to establish the driving mechanism of the instability.

[7] The paper is organized as follows. Section 2 describes the linear properties of the ion-ion kink mode as a function of various quantities. The tearing mode can coexist with the ion-ion kink mode, and thus we will compare the growth rates of the two instabilities in section 3. Summary and conclusion follow in section 4.

2. Linear Theory

2.1. Vlasov Equilibrium

[8] The equilibrium used in the linear study is the well-known Harris equilibrium [*Harris*, 1962] with several important modifications. The magnetic field is modified to include a uniform guide field

$$B_y = B_{y0}, \quad (1)$$

$$B_x = B_{x0} \tanh(z/L),$$

where L is the half thickness of the current sheet. For the hybrid simulations to be presented in paper II, we also allow for the presence of a finite normal component of the magnetic field. The magnetic field component $B_x(z)$ is produced self-consistently by the current within the sheet

$$J_y = \frac{cB_{x0}}{4\pi L} \operatorname{sech}^2\left(\frac{z}{L}\right),$$

while the B_y component of the magnetic field is externally applied. The coordinate system used is the GSM.

[9] The equilibrium distribution is modified to include a core component and a background component for both ions and electrons. In the magnetotail the core component would be the hot central plasma sheet and the background would be the cold lobe plasma. Given our interest in the magnetotail, we will use the two subscripts ‘‘h’’ (short for hot and representing the hot central plasma sheet) and ‘‘c’’ (short for cold lobe plasma) to refer to the core component

and the background population of ions and electrons respectively. In most of our parameter regimes of interest here, $T_h > T_c$ and this nomenclature is appropriate. However, in a few instances we also consider cases where the core component is colder than the background in order to get a better understanding of the instability.

[10] The core component is of the form

$$f_{cs} = \frac{n(z)}{\pi^{3/2}v_{ths}^3} \exp\left[-\frac{v_x^2 + (v_y - U_s)^2 + v_z^2}{v_{ths}^2}\right], \quad (2)$$

where $s = i, e$ for ions and electrons, $v_{ths} \equiv (2T_s/m_s)^{1/2}$ is the thermal velocity, U_s is the fluid velocity in the y -direction, T_s is the temperature, m_s is the mass, and the density profile is

$$n(z) \equiv n_h \operatorname{sech}^2\left(\frac{z}{L}\right). \quad (3)$$

The background distribution is of the form

$$f_{bs} = \frac{n_c}{\pi^{3/2}v_{ths}^3} \exp\left[-\frac{v_x^2 + v_y^2 + v_z^2}{v_{ths}^2}\right], \quad (4)$$

where n_c is background density. The equilibrium force balance imposes the constraint

$$n_h(T_e + T_h) = \frac{B_{x0}^2}{8\pi}, \quad (5)$$

and to enforce charge neutrality, one must require $U_i/T_h = -U_e/T_e$. The drift velocities are chosen to be the diamagnetic drifts resulting from the two-fluid description

$$U_s = \frac{2cT_s}{q_s B_{x0} L}. \quad (6)$$

In this manuscript the parameters characterizing the equilibrium are given in terms of dimensionless parameters. The modified Harris equilibrium is completely characterized by the following seven dimensionless numbers

$$\frac{\rho_i}{L}, \frac{m_i}{m_e}, \frac{n_c}{n_h}, \frac{T_h}{T_e}, \frac{T_c}{T_h}, \frac{B_{y0}}{B_{x0}}, \frac{\omega_{pe}}{\Omega_{ce}},$$

where $\rho_i = v_{thi}/\Omega_{ci}$ is an ion gyroradius, $v_{thi} = (2T_i/m_i)^{1/2}$ is the ion thermal speed, T_c is the temperature of the background plasma, $\Omega_{cs} = eB_{x0}/m_s c$ is the gyrofrequency computed from the asymptotic field B_{x0} and $\omega_{pe} = (4\pi n_e e^2/m_e)^{1/2}$ is the electron plasma frequency calculated from the central density n_h . The ratio of the ion fluid to thermal velocity may be expressed as $U_i/v_{thi} = \rho_i/L$, and the constraint in equation (5) permits the electron thermal velocity to be written as

$$v_{the}/c = \left[\sqrt{1 + T_h/T_e}(\omega_{pe}/\Omega_{ce})\right]^{-1}.$$

2.2. Linear Vlasov Stability

[11] The linear stability of the Vlasov equilibrium described in the previous section was calculated using the

formally exact approach described by *Daughton* [1999]. This method employs a normal mode stability calculation using a full Vlasov description for both ions and electrons. The orbit integrals arising from the linear Vlasov theory are treated numerically using the exact unperturbed particle orbits and including the form of the perturbation inside the integral. Both electromagnetic and electrostatic contributions to the field perturbation are retained and the resulting system of integrodifferential equations is solved using a basis function expansion of the eigenfunction. The addition of a guide field in the present analysis introduces a few important complications from the previous work. A new version of the linear Vlasov code was recently developed to treat the general stability problem of an arbitrary current sheet equilibrium [*Daughton*, 2003]. The results shown in the present manuscript were calculated using this new linear Vlasov code, and we refer readers to *Daughton* [2003] for a detailed description of the code. The basic strategy in this code is to perform a normal mode calculation assuming perturbations of the form

$$\hat{\phi} = \tilde{\phi}(z) \exp(-i\omega t + ik_y y + ik_x x),$$

$$\hat{A} = \tilde{A}(z) \exp(-i\omega t + ik_y y + ik_x x),$$

where $\hat{\phi}$ is the perturbed electrostatic potential and \hat{A} is the perturbed vector potential. For a given Vlasov equilibrium and for a given choice of wavenumber (k_x, k_y) , the code can compute the real frequency, growth rate (real and imaginary part of ω) and nonlocal mode structure (the complex functions $\tilde{\phi}(z)$ and $\tilde{A}(z)$). For the equilibrium discussed in section 2.1 the major instabilities are the ion-ion kink mode, the tearing instability, and the lower hybrid drift instability (LHDI). Our focus here is the ion-ion kink mode, which requires the presence of a background ion population. LHDI is suppressed in the presence of a significant background plasma ($n_e/n_h \sim 0.1$) and for $T_c/T_h \sim 1$. However, LHDI may become important for $T_c/T_h \ll 1$. Also, in the presence of a weak background ($n_e/n_h < 0.01$), LHDI has a large growth rate and its nonlinear evolution produces significant velocity shear as well as other modifications to the equilibrium [*Lapenta and Brackbill*, 2002; *Daughton*, 2002; *Lapenta et al.*, 2003]. As a result of the nonlinear changes to the profile, secondary kink type instabilities are triggered in a plain Harris sheet which share many of the same properties of the ion-ion kink instability discussed in the present manuscript. The effect of LHDI on the kink mode is beyond the scope of this paper and will be considered elsewhere. The tearing mode can coexist with the ion-ion kink mode, and we will compare the growth rates of the two instabilities in section 3.

2.3. Ion-Ion Kink Mode

2.3.1. Eigenfunction

[12] The ion-ion kink instability is a long wavelength ($k_y L \sim 1$) instability which produces a global undulation of the current sheet equilibrium. A typical example of the eigenfunction obtained from the linear Vlasov calculation is shown in Figure 1 and compared with the mode structure obtained from the 2D PIC simulations (see *Daughton* [2002] for the description of the PIC code used). In addition to perturbing the magnetic field, the

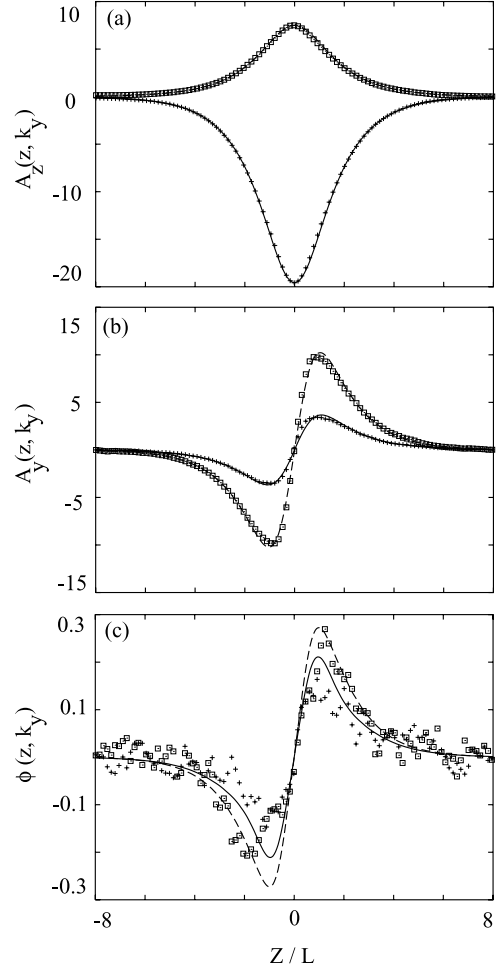


Figure 1. Comparison of ion-ion kink eigenfunction computed from linear Vlasov theory with the mode structure obtained from PIC simulation. The mode structure obtained from the simulation is represented by symbols, crosses for the cosine contribution to the Fourier series, and squares for the sine contribution. The eigenfunction obtained from linear Vlasov theory is represented by lines, solid for the cosine contribution and dashed for the sine contribution. Parameters are $\rho_i/L = 1$, $m_i/m_e = 256$, $T_h/T_e = 4$, $n_e/n_h = 0.2$, $B_{y0} = 0$, $\omega_{pe}/\Omega_{ce} = 1.66$, and $k_y L = 0.785$ and simulation time $\Omega_{ci} t = 20$.

ion-ion kink instability produces a significant electrostatic component to the field perturbation. For the parameters in Figure 1 the electrostatic contribution to the perturbed electric field $-\nabla\hat{\phi}$ is nearly equal in magnitude to the electromagnetic contribution $-(1/c)\partial A/\partial t$. In the present 2-D simulation, the tearing mode is excluded. In 3-D, the size of the electrostatic contribution may be reduced in the vicinity of the x-line.

2.3.2. Dispersion Properties

[13] Typical dispersion properties for the ion-ion kink are shown in Figure 2 for the parameters $\rho_i/L = 1$, $T_h/T_e = 5$, $B_{y0} = 0$ and $n_e/n_h = 0.2$ and at four values of the electron to ion mass ratio $m_i/m_e = 25, 100, 400, 1836$. For the fastest growing wavelength $k_y L \sim 0.7$, the results in Figure 2 are essentially independent of mass ratio for $m_i/m_e > 400$. Physically, this implies the instability is primarily an ion

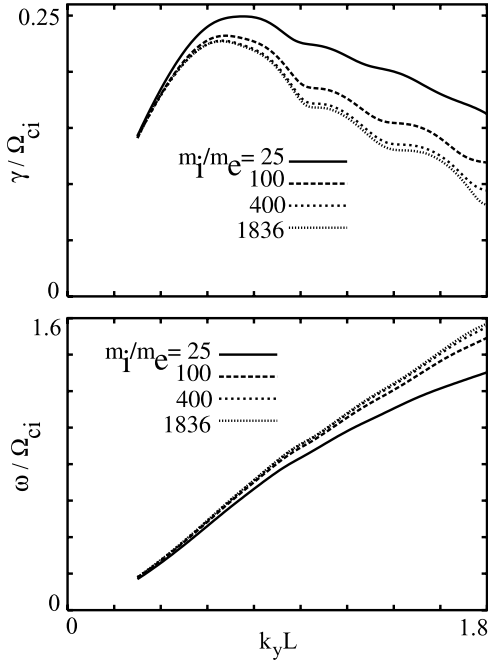


Figure 2. Typical dispersion properties for the ion-ion kink mode. Here $\rho_i/L = 1$, $T_h/T_e = 5$, $B_{y0} = 0$ and $n_c/n_h = 0.2$ and the results are shown for four values of the electron to ion mass ratio $m_i/m_e = 25, 100, 400, 1836$. For the fastest growing wavelength $k_y L \sim 0.7$, the results are essentially independent of mass ratio for $m_i/m_e > 400$.

mode and that electrons do not play an important role in the dynamics of the fastest growing mode. However, for larger values of $k_y L$ the dependence on the mass ratio becomes more significant, and it appears that an accurate treatment of this portion of the spectrum is dependent on the electron physics. The phase velocity of the ion-ion kink mode is near the bulk ion fluid velocity so that the real frequency is approximately $\omega \approx k_y U_i n_h / (n_h + n_c)$. For thicker current sheets $\rho_i/L \sim 0.2$, the wavelength of maximum growth shifts to shorter wavelength $k_y L \sim 1.2-1.8$ depending on the background component n_c/n_h .

2.3.3. ρ_i/L Dependence

[14] The driving factor for the ion-ion kink instability will be addressed in paper II. The two sources of free energy are ion-ion streaming and velocity shear. Recall that the ion fluid velocity of the main component is related to the sheet thickness by $U_i/v_{thi} = \rho_i/L$, and thus the relative streaming velocity between the primary and background ion distributions is simply proportional to ρ_i/L . Although a standard Harris equilibrium has no velocity shear, the addition of a uniform background produces a velocity shear that is also proportional to ρ_i/L . This can be seen by using a single fluid description of the problem obtained by summing over the two ion components. In this single fluid description, the velocity profile of the bulk fluid is

$$U_{fluid}(z) = \frac{n(z)U_i}{n(z) + n_c}, \quad (7)$$

where U_i is the uniform Harris drift velocity, $n(z)$ is the Harris density given in equation (3), and n_c is the density of

uniform background. The question of the relative importance of these two potential driving factors will be addressed in the next section. Regardless of which driving factor is dominant, both the relative ion streaming and the velocity shear increase as ρ_i/L increases (i.e., as the current sheet becomes thinner). The growth rate, wave number, and real frequency obtained from the linear Vlasov code are shown in Figure 3 as a function of ρ_i/L . The physical parameters are $n_c/n_h = 0.20$, $T_h = T_e$, $m_i/m_e = 256$, and $B_{y0} = 0$, and we have scanned the wavelength to find the maximum growth in each case. The fastest growing mode goes to significantly shorter wavelength for thicker sheets as shown in Figure 3. As expected, the growth rate is a strongly increasing function of ρ_i/L . The real frequency in Figure 3 corresponds approximately to the functional form $\omega/\Omega_{ci} \approx k_y L (\rho_i/L)^2 / (1 + n_c/n_h)$ since the phase velocity of the mode is approximately equal to the single fluid velocity near the central region $\omega/k_y \approx U_{fluid}(x = 0)$. Although the growth rate is significantly reduced for thick sheets, the ion-ion kink maintains a growth rate which is always significantly greater than the tearing mode (see section 3).

2.3.4. Dependence on Background Density n_c

[15] The dependence of the growth rate and real frequency of the ion-ion kink instability as a function of background density is shown in Figure 4 for the parameters $\rho_i/L = 1$, $T_h = T_e$, $m_i/m_e = 256$, and $B_{y0} = 0$. The wavelength is held fixed at $k_y L = 0.7$ which corresponds to the fastest growing mode for most of the range of background densities. At very low background density $n_c/n_h < 0.01$,

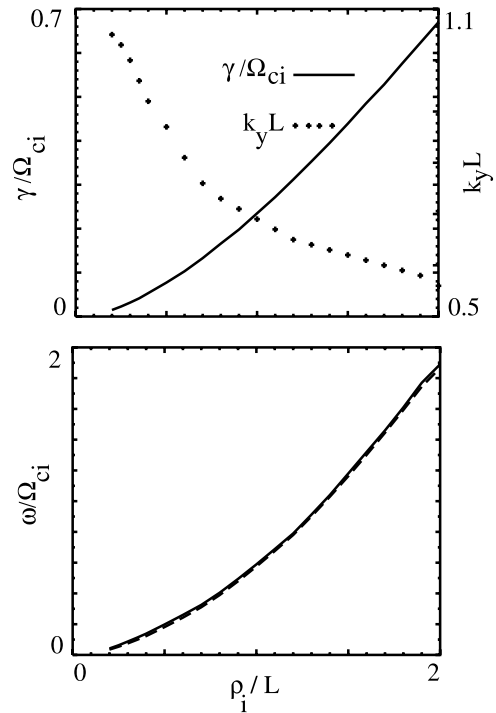


Figure 3. Growth rate, the wave number of maximum growth, and real frequency of the kink instability as a function of sheet thickness ρ_i/L for the parameters $m_i/m_e = 256$, $T_h = T_e$, $n_c/n_h = 0.2$, $B_{y0} = 0$, $\omega_{pe}/\Omega_{ce} = 3$. The dashed line in the bottom figure corresponds to $\omega/\Omega_{ci} = k_y L (\rho_i/L)^2 / (1 + n_c/n_h)$.

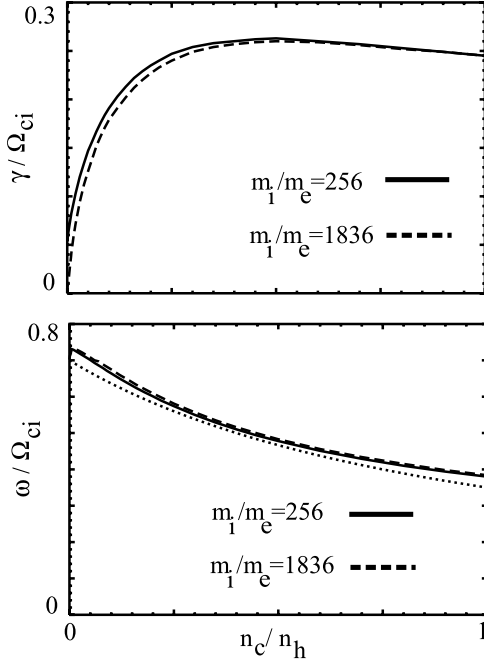


Figure 4. Growth rate and real frequency of the kink instability as a function of background density n_c/n_o for the parameters $\rho_i/L = 1$, $T_h = T_e$, $B_{y0} = 0$, $\omega_{pe}/\Omega_{ce} = 3$ and $k_y L = 0.70$ which corresponds approximately to the fastest growing wavelength. Results are presented for two values of the mass ratio $m_i/m_e = 256, 1836$. The dotted line in the bottom figure corresponds to $\omega/\Omega_{ci} = k_y L (\rho_i/L)^2 / (1 + n_c/n_h)$.

the fastest growing mode shifts to slightly longer wavelength $k_y L \sim 0.6$ but the change to the growth rate is relatively small. The finite growth rate for the limit $n_c = 0$ corresponds to the drift kink mode of a Harris sheet [Daughton, 1999]. In this limit, there is no ion-ion streaming or velocity shear so that the only remaining driving factor is the relative streaming between electrons and ions in the current sheet. In the limit of realistic mass ratio, the growth rate of the drift kink mode becomes very weak. The obvious question is whether the presence of a background introduces a new unstable mode to the system or merely enhances the weak drift-kink mode. The form of the eigenfunction, the real frequency and the growth rate all indicate that the transition between the limit $n_c = 0$ (drift kink instability) and the case of finite background density (ion-ion kink instability) is continuous. In other words, it does not appear that introducing a background gives rise to a new eigenmode of the system, rather the presence of ion-ion streaming and ion velocity shear merely enhance the growth rate of the existing eigenmode (drift kink).

[16] For a background density larger than $n_c/n_h > 0.05$, the ion-ion kink instability is essentially an ion mode and is nearly independent of the ratio of the electron to ion temperature. As an example, for $n_c/n_h = 0.2$, the variation in the real frequency and growth rate over the range $0.1 < T_h/T_e < 10$ is less than a few percent. However, in the limit of very low background density $n_c < 0.01$ the mode begins to recover some of the dependence on T_i/T_e observed for the drift kink instability [Daughton, 1999]. In the limit of no background, the only source of free energy is the relative

drift between electrons and ions which is constrained by the relation $U_h/T_h + U_e/T_e = 0$. This imposes a strong dependence on T_h/T_e in the limit of $n_c \rightarrow 0$ as discussed by Daughton [1999].

2.3.5. T_c Dependence

[17] The dependence of the growth rate and real frequency on the background temperature T_c/T_h is shown in Figure 5 for the parameters $n_c/n_h = 0.2$, $m_i/m_e = 256$, $T_h = T_e$, $k_y L = 0.7$ and for three values of the sheet thickness. Here we consider cases where $T_c > T_h$ in order to gain insight into the properties of the ion-ion mode. In this section the nomenclature “c” and “h”, which we use to refer to the cold lobe and hot plasma sheet ions in the magnetotail, are not appropriate. However rather than introduce a new nomenclature, we just point out that in this section “c” and “h” are to be understood as referring to the background and core plasma populations, respectively.

[18] In this comparison the temperature of both the background ions and background electrons is T_c , although the results are nearly independent of the electron temperature for this background density. Since the bulk fluid velocity in equation (7) is completely independent of the background temperature, the results in Figure 5 offer strong evidence that the ion kink instability is not a simple Kelvin-Helmholtz instability. The linear Vlasov code predicts that the ion kink mode is enhanced if the background population is colder than the Harris population of ions $T_c/T_h < 1$ or alternatively if the background population is significantly hotter $T_c/T_h > 6$. For the intermediate range of background temperatures the growth rate is significantly reduced relative to the case of equal temperature $T_c = T_h$ and a minimum

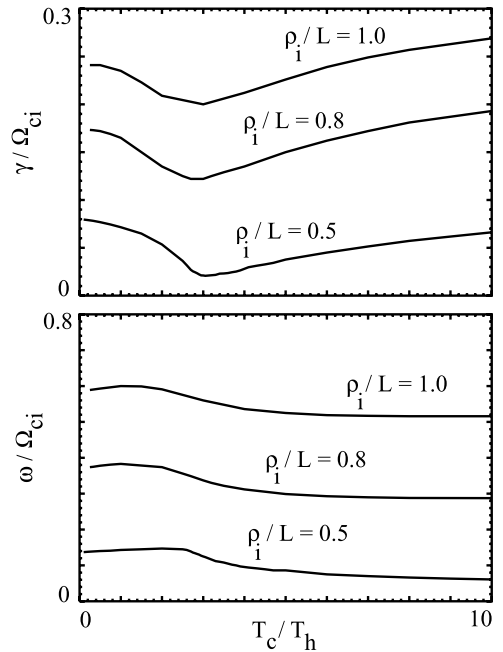


Figure 5. Growth rate and real frequency of the kink instability as a function of background temperature T_c/T_h for the parameters $n_c/n_h = 0.2$, $m_i/m_e = 256$, $T_h = T_e$, $B_{y0} = 0$, $\omega_{pe}/\Omega_{ce} = 3$, $k_y L = 0.7$ and for three values of the sheet thickness $\rho_i/L = 0.5, 0.8, 1.0$. The ions and electrons in the background plasmas both have temperature T_b .

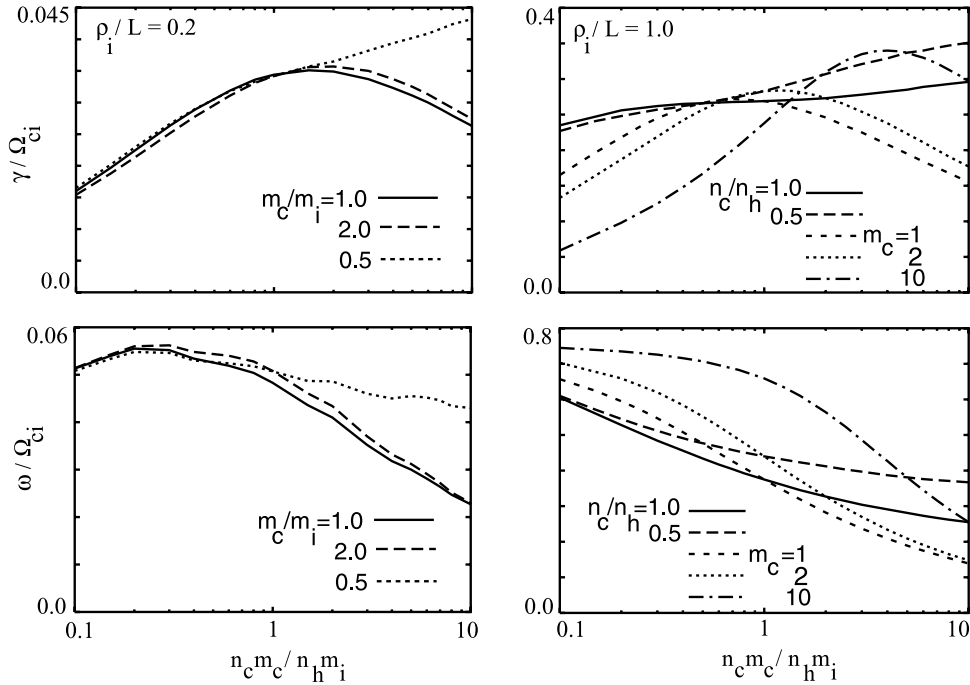


Figure 6. Growth rate and real frequency of the kink instability as a function of mass density of the background ions for two different current sheet thicknesses. The parameters for the left panels are $\rho_i/L = 0.2$, $T_h = T_c$, $T_c/T_h = 0.02$, $m_i/m_e = 256$, and $B_{y0} = 0$. The k_y is chosen to correspond to the maximum growth at each mass density. The parameters for the right panel are $\rho_i/L = 1$, $n_c/n_h = 0.2$, and $m_i/m_e = 256$. In this case, $k_y L = 0.7$ and is kept fixed.

growth rate is found near $T_c/T_h \sim 3$. Although we are merely speculating, it seems that the likely mechanism responsible for these results involves a kinetic interaction between the background ions and the mode. In the cold limit most of the background ions are strongly magnetized with a gyroradius small in comparison to the sheet thickness so that kinetic interactions between the background ions and the mode are minimized. However, for the case of warmer background ions $T_c > T_h$, the gyroradius of the noncrossing background ions is larger and a significant fraction of the ions follow meandering orbits, crossing both sides of the sheet. The phase velocity of the mode $\omega/k_y \approx U_i n_h / (n_h + n_c)$ is in the proper range for resonant wave particle interaction with the meandering ions. It appears that these types of kinetic effects lead to a fairly significant damping of the mode for $T_c/T_h \sim 3$. However, at larger background temperature $T_c/T_h > 6$, the kinetic interaction with meandering background ions appears to be destabilizing. More work is needed to fully understand the essential physics responsible for this trend. Nevertheless, it is clear that the properties of the ion kink instability have dependencies on the details of the ion distribution in a way that makes it different from the standard Kelvin-Helmholtz instability.

2.3.6. Mass Density Dependences

[19] In order to gain more insight into the driving factor of the ion-ion kink instability, we contrast it with the Kelvin-Helmholtz instability (KHI). In KHI, a denser or heavier background accelerates growth and the growth rate has a dependence of the form $\gamma \propto (v_2 - v_1) (\rho_{m1} \rho_{m2})^{1/2} / (\rho_{m1} + \rho_{m2})$ [e.g., Melrose, 1986]. Here, the indices 1, 2 refer to quantities on the two sides of a discontinuous flow, and ρ_m is the mass density. Interpreting the two “sides” as the central

current-carrying ions and the lobe ions, respectively, we have examined how well the ion-ion kink mode follows this expression. This is illustrated in Figure 6, which shows the growth rate and frequency as a function of mass density using different combinations of n_c and m_c and for two different current sheet thicknesses. The parameters for the left panel are $\rho_i/L = 0.2$, $T_h = T_c$, $T_c/T_h = 0.02$, $m_i/m_e = 256$, and $B_{y0} = 0$. For each value of the mass density, we have scanned over k_y to find the maximum growth rate. At mass density 0.1, the maximum growth is at $k_y L = 1.17$ while at mass density 10.0 the maximum growth is at $k_y L = 1.80$. For mass density of ≤ 1 , all three curves are closely matched, suggesting a close relation to the KHI. For mass densities larger than 1, the curve for a fixed density but varying mass deviates from the other two curves. This may be due to the deviations of the mode properties from the simple fluid picture for such heavy cold ions. The right panel shows the results for a thin sheet, $\rho_i/L = 1$, $T_h = T_c$, $T_c/T_h = 0.02$, $m_i/m_e = 256$, and $B_{y0} = 0$. In this case we have kept $k_y L = 0.7$ which is near the maximum growth for a thin sheet. In this case, the mode properties clearly are more complex than the simple expression stated above for the KHI. This is not too surprising since for such thin sheets kinetic effects become important and some of the differences may be attributed to the fact that the above growth rate expression assumes that the background population is fully magnetized. If we increase the background mass while holding the background density fixed, this population becomes unmagnetized when the growth rate of the mode is much larger than the ion cyclotron frequency of the background ions. This is why the growth rate is not suppressed for large m_c (holding n_c fixed) since the

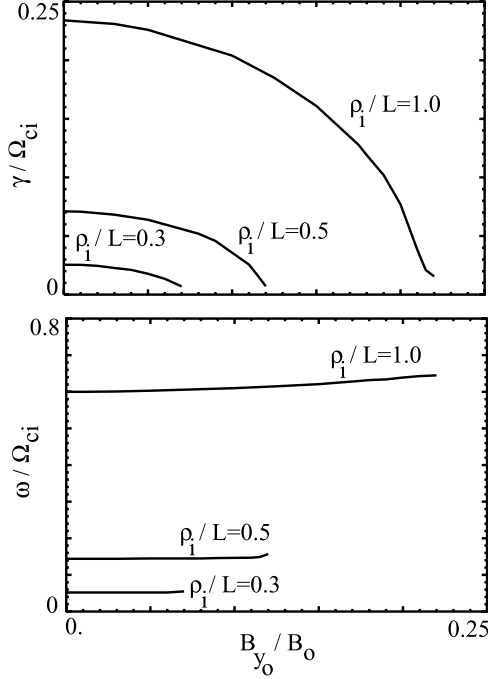


Figure 7. Growth rate and real frequency of the kink instability as a function of guide field B_{y0}/B_{x0} for the parameters $\rho_1/L = 1$, $n_c/n_h = 0.2$, $m_i/m_e = 256$, $T_h = T_c$, $\omega_{pe}/\Omega_{ce} = 3$, $k_y L = 0.7$, and for three values of the sheet thickness.

perturbation is too fast for these heavy ions to respond. On the other hand, if we fix $m_c = 1$ and increase n_c , then the background population is magnetized and will “feel” the perturbation so that for large n_c the mode is suppressed. However, even for m_c as large as 10, the growth rate still has a maximum, albeit pushed further out in terms of mass density, and then decreases. This is because the heavy ions “feel” the perturbation to some small degree and are not truly unmagnetized. So as we add more and more heavy ions, it eventually drags down the mode. As the growth rate begins to decrease, the heavy ions become more magnetized so it slows down the mode even faster.

2.3.7. T_h/T_e Dependence

[20] We have calculated the linear properties as a function of the electron to ion (hot central plasma sheet) temperature for both a thick and a thin sheet. In both cases we have found the dependence on this ratio to be very weak. This is expected since the ion-ion kink mode is an ion mode and should be insensitive to details of electron physics.

2.3.8. Guide Field B_{y0} Dependence

[21] All results presented thus far have been for the case of zero guide field $B_{y0} = 0$. In this limit, the ion kink instability gives rise to a global undulation of the current sheet but does not bend magnetic field lines. The equilibrium Harris field and the resulting magnetic perturbation are both entirely in the x direction. It should be immediately clear that the introduction of a guide field is strongly stabilizing to the ion kink mode since bending of the equilibrium magnetic field is necessary. In the presence of a guide field, all three components of the magnetic field are perturbed. The stabilizing influence of the guide field is shown in Figure 7 for the parameters $\rho_1/L = 1$, $n_c/n_h = 0.2$,

$m_i/m_e = 256$ and $k_y L = 0.7$. For this case the mode is completely stabilized for guide fields larger than $B_{y0}/B_{x0} > 0.22$. For certain instabilities the introduction of a guide field will cause the fastest growing mode to rotate to an oblique angle so that $\mathbf{k} \times \mathbf{B} = 0$ in the region where the driving factor is maximum. In the case of the lower hybrid instability, the driving factor is the density gradient on the edge of the sheet, so that the introduction of a guide field causes the fastest growing mode to rotate such that $\mathbf{k} \times \mathbf{B} = 0$ in this region. However, the fastest growing ion kink mode always occurs for $k_x = 0$ regardless of the magnitude of the guide field. This is not necessarily what one would expect if the primary driving factor for the ion kink mode were velocity shear, which is maximum on the edge of the sheet. However, this result is consistent with ion-ion streaming as the dominant driving factor since the density of the main ion population with drift U_i is strongly peaked in the central region where $B_x \approx 0$. For all values of the guide field the eigenfunction is always clearly localized about the central region, so that it is not possible to pick a k_x such that $\mathbf{k} \times \mathbf{B} = 0$.

3. Tearing Mode

[22] The growth rate of the tearing mode is shown in Figure 8 for the parameters $\rho_1/L = 1$, $T_h/T_e = 5$, $n_c/n_h = 0.2$, and $B_{y0} = 0$ and at four values of the electron to ion mass ratio $m_i/m_e = 25, 100, 400$, and 1836. The fastest growing wavelength is $k_x L \sim 0.5$, although this appears to shift to slightly longer wavelength at realistic mass ratio. For parameter regimes of interest in this work the growth rate of the tearing mode is considerably weaker than the ion-ion kink instability.

[23] We have calculated the maximum growth rate of the tearing mode as a function of mass of the background ions relative to the mass of the equilibrium ions (m_c/m_i) for two different current sheet thicknesses (ρ_1/L) of 0.5 and 1.0. The background ion temperature is kept fixed. We find a very weak dependence: for $\rho_1/L = 0.5$ the growth rate γ/Ω_{ci} varies from 0.01 to 9.17×10^{-3} when changing m_c/m_i the from 0 to 16. Similarly for $\rho_1/L = 1.0$ the γ/Ω_{ci} varies from 0.0475 to 0.044 when changing m_c/m_i the from 0 to 16. The other parameters in these calculations were $T_c/T_e = 5$, $n_c/n_h = 0.1$,

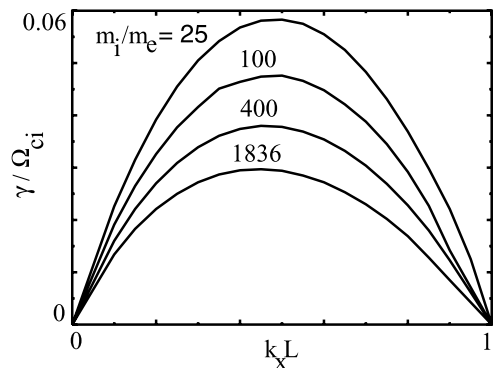


Figure 8. Growth rate of the tearing instability as a function of wavelength for the parameters $\rho_1/L = 1$, $T_h/T_e = 5$, $n_c/n_h = 0.2$, $B_{y0} = 0$ and at mass ratios $m_i/m_e = 25, 100, 400$, and 1836.

$T_c/T_h = 0.06$, and $m_i/m_e = 256$. In the linear regime the presence of a background ion population affects the growth rate of the tearing mode based on the additional number of resonant particles that it introduces. The growth rate shows a small increase with the mass of the background ions because the number of resonant particles is reduced for heavier ions. The effective number of resonant particles is more directly affected with changing background temperature and density. That is why the tearing mode is a sensitive function of the background ion temperature and density but insensitive to the mass of the background ions. This is in contrast to the ion-ion kink mode which has a strong dependence on the mass of the background ions (section 2.3.6). We should point out, however, that although the observed increase with mass is very weak in the linear regime, in the nonlinear regime the mass dependence, which controls the Alfvén speed, may play a more important role.

4. Summary

[24] We have performed a detailed study of the linear properties of the ion-ion kink mode. The ion-ion kink instability is a long wavelength ($k_y L \sim 1$) instability which produces a global undulation of the current sheet equilibrium. The instability is primarily an ion mode and the electrons do not play an important role in the dynamics of the fastest growing mode. Although the growth rate is significantly reduced for thick sheets, for a modest lobe density the ion-ion kink maintains a growth rate which is always significantly greater than the tearing mode and is thus expected to be prevalent in the magnetotail. The two sources of free energy available for driving the ion-ion mode are ion-ion streaming and velocity shear. Although linear theory results indicate strong similarities to the standard Kelvin-Helmholtz instability, the mode exhibits dependencies on the details of the ion distribution in a way that makes it different from the standard Kelvin-Helmholtz instability. For instance the growth rate of the mode varies as a function of the background temperature whereas the bulk fluid velocity (a measure of the velocity shear) is independent of the background temperature. Also we compared the growth rate dependencies of the ion-ion mode against that for the KHI which has the form $\gamma \propto (v_2 - v_1) (\rho_{m1} \rho_{m2})^{1/2} / (\rho_{m1} + \rho_{m2})$ [e.g., Melrose, 1986]. We found a more complex dependency of the growth rate of the ion-ion kink mode than this simple expression. A strong guide field can stabilize the ion-ion kink mode but otherwise this mode appears to be quite robust, retaining significant growth rate under a variety of conditions and is expected to be prevalent in the magnetotail. Given the presence of multiple ion populations at the magnetopause, the ion-ion kink mode may also be active in the magnetopause current layer and a study of the mode for these parameter regimes may prove interesting.

[25] **Acknowledgments.** The research of H. Karimabadi and D. Krauss-Varban was supported by NASA SEC Theory Program NAG5-11754 and NSF grant ATM-9901665. The research of P. Pritchett was supported by NASA grant NAG 5-10287. The research of W. Daughton was supported by the LDRD program at Los Alamos National Laboratory.

[26] Lou-Chuang Lee thanks Joseph Huba and Shui Wang for their assistance in evaluating this paper.

References

- Chang, C. L., H. K. Wong, and C.-S. Wu, Electromagnetic instabilities attributed to a cross-field ion drift, *Phys. Rev. Lett.*, **65**, 1104, 1990.
- Daughton, W., Kinetic theory of the drift kink instability in a current sheet, *J. Geophys. Res.*, **103**, 29,429, 1998.
- Daughton, W., The unstable eigenmodes of a neutral sheet, *Phys. Plasmas*, **6**, 1329, 1999.
- Daughton, W., Nonlinear dynamics of thin current sheets, *Phys. Plasmas*, **9**, 3668, 2002.
- Daughton, W., Electromagnetic properties of the lower-hybrid drift instability in a thin current sheet, *Phys. Plasmas*, **10**, 3103, 2003.
- Davidson, R. C., and N. T. Gladd, Anomalous transport properties associated with the lower-hybrid-drift instability, *Phys. Fluids*, **18**, 1327, 1975.
- Drake, J. F., R. G. Kleva, and M. E. Mandt, Structure of thin current layers: Implications for magnetic reconnection, *Phys. Rev. Lett.*, **73**, 1251, 1994.
- Drake, J. F., D. Biskamp, and A. Zeiler, Breakup of the electron current layer during 3-D collisionless magnetic reconnection, *Geophys. Res. Lett.*, **24**, 2921, 1997.
- Fuselier, S. A., Kinetic aspects of reconnection at the magnetopause, in *Physics of the Magnetopause*, *Geophys. Monogr. Ser.*, vol. 90, edited by P. Song, B. U. O. Sonnerup, and M. F. Thomsen, AGU, Washington, D.C., 1995.
- Galeev, A.-A., and L.-M. Zelenyi, Tearing instability in plasma configuration, *Sov. Phys. JETP*, Engl. Transl., **43**, 1113, 1976.
- Harris, E. G., On a plasma sheath separating regions of oppositely directed magnetic field, *Nuovo Cimento*, **23**, 116, 1962.
- Hesse, M., and J. Birn, Near- and mid-tail current flow during substorms: Small- and large-scale aspects of current disruption, in *Magnetospheric Current Systems*, *Geophys. Monogr. Ser.*, vol. 118, edited by S. Ohtani et al., p. 295, AGU, Washington, D.C., 2000.
- Huba, J. D., N. T. Gladd, and K. Papadopoulos, The lower-hybrid-drift instability as a source of anomalous resistivity for magnetic field line reconnection, *Geophys. Res. Lett.*, **4**, 125, 1977.
- Huba, J. D., J. F. Drake, and N. T. Gladd, Lower-hybrid-drift instability in field reversed plasmas, *Phys. Fluids*, **23**, 552, 1980.
- Karimabadi, H., P. L. Pritchett, W. Daughton, and D. Krauss-Varban, Ion-ion kink instability in the magnetotail: 2. Three-dimensional full particle and hybrid simulations and comparison with observations, *J. Geophys. Res.*, **108**, doi:10.1029/2003JA010109, in press, 2003.
- Kaufmann, R. L., Substorm currents: Growth phase and onset, *J. Geophys. Res.*, **92**, 7471, 1987.
- Krauss-Varban, D., and H. Karimabadi, Timing and localization of reconnection signatures: Is there a substorm model problem?, *Geophys. Res. Lett.*, **30**, doi:10.1029/2002GL016369, in press, 2003.
- Krauss-Varban, D., and N. Omid, Incorporating the near-Earth region in large-scale hybrid simulations of the magnetotail, *Eos Trans. AGU*, **77**(44), Fall Meet. Suppl., F617, 1996.
- Lapenta, G., and J. U. Brackbill, Nonlinear evolution of the lower hybrid drift instability: Current sheet thinning and kinking, *Phys. Plasmas*, **9**, 1544, 2002.
- Lapenta, G., J. U. Brackbill, and W. Daughton, The unexpected role of the lower hybrid drift instability in magnetic reconnection in three dimensions, *Phys. Plasmas*, **10**, 1577, 2003.
- Lin, N., R. L. McPherron, M. G. Kivelson, and R. J. Walker, Multipoint reconnection in the near-Earth magnetotail: CDAW 6 observations of energetic particles and magnetic field, *J. Geophys. Res.*, **96**, 19,427, 1991.
- Lui, A. T. Y., Inferring global characteristics of current sheet from local measurements, *J. Geophys. Res.*, **98**, 13,423, 1993.
- Lui, A. T. Y., A. Mankofsky, C.-L. Chang, K. Papadopoulos, and C.-S. Wu, A current disruption mechanism in the neutral sheet: A possible trigger for substorm expansions, *Geophys. Res. Lett.*, **17**, 745, 1990.
- Lui, A. T. Y., C.-L. Chang, A. Mankofsky, H.-K. Wong, and D. Winske, A cross-field current instability for substorm expansions, *J. Geophys. Res.*, **96**, 11,389, 1991.
- McPherron, R. L., A. Nishida, and C. T. Russell, Is near-Earth current sheet thinning the cause of auroral substorm onset?, in *Quantitative Modeling of Magnetosphere-Ionosphere Coupling Processes*, edited by Y. Kamide and R.-A. Wolf, p. 252, Kyoto Sangyo Univ., Kyoto, Japan, 1987.
- Melrose, D. B., *Instabilities in Space and Laboratory Plasmas*, Cambridge Univ. Press, New York, 1986.
- Mitchell, D. G., D. J. Williams, C. Y. Huang, L. A. Frank, and C. T. Russell, Current carriers in the near-Earth cross-tail current sheet during substorm growth phase, *Geophys. Res. Lett.*, **17**, 583, 1990.
- Miura, A., S. Ohtani, and T. Tamao, Ballooning instability and structure of diamagnetic hydromagnetic waves in a model magnetosphere, *J. Geophys. Res.*, **94**, 15,231, 1989.

- Ozaki, M., T. Sato, R. Horiuchi, and The Complexity Simulation Group, Electromagnetic instability and anomalous resistivity in a magnetic neutral sheet, *Phys. Plasmas*, 3, 2265, 1996.
- Pritchett, P. L., F. V. Coroniti, and V. K. Decyk, Three-dimensional stability of thin quasi-neutral current sheets, *J. Geophys. Res.*, 101, 27,413, 1996.
- Pulkkinen, T. I., D. N. Baker, R. J. Pellinen, J. Buchner, H. E. J. Koskinen, R. E. Lopez, R. L. Dyson, and L. A. Frank, Particle scattering and current sheet stability in the geomagnetic tail during the substorm growth phase, *J. Geophys. Res.*, 97, 19,283, 1992.
- Pulkkinen, T. I., D. N. Baker, L. L. Cogger, L. A. Frank, J. B. Sigwarth, S. Kokubun, T. Mukai, H. J. Singer, J. A. Slavin, and L. Zelenyi, Spatial extent and dynamics of a thin current sheet during the substorm growth phase on December 10, 1996, *J. Geophys. Res.*, 104, 28,475, 1999.
- Roux, A., Generation of field-aligned current structures at substorm onsets, in *Proceedings of ESA Workshop on Future Missions in Solar, Heliospheric, and Space Plasma Physics, Spec. Publ. ESA SP-235*, p. 151, Eur. Space Agency, Paris, 1985.
- Roux, A., S. Perraut, P. Robert, A. Morane, A. Pedersen, A. Korth, G. Kremser, B. Aparicio, D. Rodgers, and R. Pellinen, Plasma sheet instability related to the westward traveling surge, *J. Geophys. Res.*, 96, 17,697, 1991.
- Russell, C. T., The structure of the magnetopause, in *Physics of the Magnetopause, Geophys. Monogr. Ser.*, vol. 90, edited by P. Song, B. U. O. Sonnerup, and M. F. Thomsen, p. 91, AGU, Washington, D.C., 1995.
- Schindler, K., A theory of the substorm mechanism, *J. Geophys. Res.*, 79, 2803, 1974.
- Sergeev, V. A., P. Tanskanen, K. Mursula, A. Korth, and R. C. Elphic, Current sheet thickness in the near-Earth plasma sheet during substorm growth phase, *J. Geophys. Res.*, 95, 3819, 1990.
- Sergeev, V. A., D. G. Mitchell, C. T. Russell, and D. J. Williams, Structure of the tail plasma/current sheet at $\sim 11R_E$ and its changes in the course of a substorm, *J. Geophys. Res.*, 98, 17,345, 1993.
- Sergeev, V., A. Runov, W. Baumjohann, R. Nakamura, T. L. Zhang, M. Volwerk, A. Balogh, H. Reme, J. A. Sauvaud, M. Andre, and B. Klecker, Current sheet flapping motion and structure observed by Cluster, *Geophys. Res. Lett.*, 30(6), 1327, doi:10.1029/2002GL016500, 2003.
- Song, P., et al., Structure and properties of the subsolar magnetopause for northward interplanetary magnetic field: Multiple-instrument particle observations, *J. Geophys. Res.*, 98, 11,319, 1993.
- Volwerk, M., K.-H. Glassmeier, A. Runov, W. Baumjohann, R. Nakamura, T. L. Zhang, B. Klecker, A. Balogh, and H. Reme, Kink mode oscillation, *Geophys. Res. Lett.*, 30(6), 1320, doi:10.1029/2002GL016467, 2003.
- Yoon, P. H., J. F. Drake, and A. T. Y. Lui, Theory and simulation of Kelvin-Helmholtz instability in the geomagnetic tail, *J. Geophys. Res.*, 101, 27,327, 1996.
- Zhu, Z., and R. M. Winglee, Tearing instability, flux ropes, and the kinetic current sheet kink instability in the Earth's magnetotail: A three-dimensional perspective from particle simulations, *J. Geophys. Res.*, 101, 4885, 1996.

W. Daughton, Plasma Physics Group X-1, Los Alamos National Laboratory, Los Alamos, NM 87545, USA. (daughton@lanl.gov)

H. Karimabadi and D. Krauss-Varban, Department of Electrical and Computer Engineering, University of California, San Diego, Mail Code 0407, La Jolla, CA 92093-0407, USA. (homa@ece.ucsd.edu; varban@ece.ucsd.edu)

P. L. Pritchett, Department of Physics and Astronomy, University of California, Los Angeles, Los Angeles, CA 90095-1547, USA. (pritchet@physics.ucla.edu)